Machine Learning Potential for Electrochemical Interfaces with Hybrid Representation of Dielectric Response

Jia-Xin Zhu*
State Key Laboratory of Physical Chemistry of Solid Surfaces, iChEM, College of Chemistry and Chemical Engineering, Xiamen University, Xiamen 361005, China

Jun Cheng†
State Key Laboratory of Physical Chemistry of Solid Surfaces, iChEM, College of Chemistry and Chemical Engineering, Xiamen University, Xiamen 361005, China and Laboratory of AI for Electrochemistry (AI4EC), IKKEM, Xiamen 361005, China and Institute of Artificial Intelligence, Xiamen University, Xiamen 361005, China

(Received 4 November 2024; accepted 6 June 2025; published 2 July 2025)

Understanding electrochemical interfaces at a microscopic level is essential for elucidating important electrochemical processes in electrocatalysis, batteries, and corrosion. While *ab initio* simulations have provided valuable insights into model systems, the high computational cost limits their use in tackling complex systems of relevance to practical applications. Machine learning potentials offer a solution, but their application in electrochemistry remains challenging due to the difficulty in treating the dielectric response of electronic conductors and insulators simultaneously. In this Letter, we propose a hybrid framework of machine learning potentials that is capable of simulating metal-electrolyte interfaces by unifying the interfacial dielectric response accounting for local electronic polarization in electrolytes and nonlocal charge transfer in metal electrodes. We validate our method by reproducing the bell-shaped differential Helmholtz capacitance at the Pt(111)-electrolyte interface. Furthermore, we apply the machine learning potential to calculate the dielectric profile at the interface, providing new insights into electronic polarization effects. Our Letter lays the foundation for atomistic modeling of complex, realistic electrochemical interfaces using machine learning potential at *ab initio* accuracy.

DOI: 10.1103/48ct-3jxm

Electrochemistry underpins critical processes in material synthesis [1,2], energy conversion [3,4], and storage [5]. However, our understanding of electrochemical interfaces, where these reactions occur, remains limited [6]. Atomistic modeling offers microscopic insights but often struggles to balance accuracy and computational efficiency. Accurate descriptions of interfacial phenomena, such as pH- and potential-dependent hydrogen bonding networks [7–10], require explicit treatment of electronic structures. For instance, water chemisorption on Pt can induce electron redistribution at the interface, affecting water structure and the electric double layer (EDL) capacitance [11]. While *ab initio* molecular dynamics (AIMD) captures both electronic and molecular dynamics, its high cost restricts simulations to systems of hundreds of atoms at the timescale of tens of picoseconds [12].

Fortunately, emerging machine learning (ML) techniques offer a promising alternative, maintaining *ab initio* accuracy with significantly reduced computational demand [13–16]. ML potentials (MLPs) accelerate simulations by 10^3–10^5 times compared to density functional theory (DFT) and scale almost linearly with system size [17,18], making slow processes in systems with complex structures tractable [19–21]. Even solvated electrons can be effectively modeled as "ghost" atoms using MLPs, yielding accurate structural and dynamical properties [22].

Despite recent progress, applying MLPs in electrochemistry remains challenging. Most MLPs are short ranged due to finite cutoffs (typically ≤ 8 Å) in descriptor construction [15,23,24], which limits their applicability in systems with long-range interactions. While short-range MLPs can describe neutral metal-water interfaces, likely originating from the high dielectric constant of water in the zero-field limit [25,26], they might fail to maintain electroneutrality in bulk electrolytes when ions are present in the system [27]. To address this, several approaches incorporate long-range interactions by decomposing the total energy into short- and long-range contributions. The long-range part, often approximated as electrostatic interactions, is computed analytically, while the short-range part is predicted using standard MLPs [28–30]. Although this decomposition is somewhat artificial, it has achieved *ab initio* accuracy in describing

*Contact author: jiaxinzhu@stu.xmu.edu.cn
†Contact author: chengjun@xmu.edu.cn

thermodynamic and dynamic properties in a variety of systems [27,30,31]. Alternatively, long-range effects also can be embedded directly into the descriptors [32].

In addition to incorporating long-range interactions, another major challenge is accurately representing dielectric response, which is essential for modeling interfacial polarization under specific electrostatic boundary conditions. Some recent models incorporate electronic polarization based on local chemical environments [30,31,33–35]. These are suitable for insulators but inadequate for metallic systems involving nonlocal charge transfer, due to the shortsightedness of the descriptors. To overcome this, charge equilibration (QEq)-based MLPs have been proposed [29,36,37], which allow nonlocal charge redistribution. However, these models inherit the limitations of the QEq scheme, including semilocal approximations of kinetic energy. As a result, they tend to overestimate the polarizability of insulators and incorrectly predict fractional charges upon molecular dissociation, limiting their applicability to isolated molecules or clusters [38–40].

In this Letter, we propose a hybrid scheme of MLPs to treat electrochemical interfaces (ec-MLP), which integrates the dielectric responses of electronically insulating electrolytes and conducting metal electrodes. The feasibility of the ec-MLP proposed in this Letter is illustrated in an important and challenging model system, i.e., the Pt(111)-KF(aq) interfaces. For this model system, the ec-MLP can describe not only the water chemisorption phenomenon but also the potential-dependent interfacial structures and differential capacitances. Based on the well-validated ec-MLP, we further calculate the dielectric profile at the Pt-water interface, which reveals the importance of electronic effects and offers new insights into the molecular origins of interfacial dielectric properties.

In the electronically insulating electrolyte, the dielectric response is mainly undertaken by the motion of atoms and ions. We therefore choose the Wannier centroid (WC) method to describe this dielectric response, which, from a theoretical perspective, allows reasonable descriptions of both thermodynamic and transport properties (see Supplemental Material [41] for more details). The WC is defined following Ref. [97], with its position relative to the associated nucleus predicted from the local chemical environment. This is a reasonable approximation considering the minor effect of electric fields on frozen electrolyte configurations [98]. Nevertheless, this secondary effect can be further incorporated by introducing polarizability terms [30]. In contrast, dielectric response in metallic electrodes is dominated by electronic polarization. Several models have been developed to describe this electronic dielectric response, commonly referred to as the polarizable electrode approach [99–102]. Among them, the Siepmann-Sprik model [100], which can be regarded as a specific case of the QEq scheme (see Supplemental Material [41] for more details), is particularly notable for its wide application. It approximates the charge distributions with spherical Gaussian charges centered on atomic sites of electrodes, yielding a quadratic electrostatic energy functional of atomic charges. The optimal charge distribution, obtained by minimizing this energy, adapts to changes in atomic configurations and boundary conditions, effectively capturing the electronic dielectric response. Remarkably, the Siepmann-Sprik model has been integrated into hybrid quantum mechanics/molecular mechanics frameworks [103], where it successfully reproduces both long-range interactions and adsorption energies consistent with full DFT calculations. The promising result indicates that the Siepmann-Sprik model is a good choice for describing the electronic dielectric response of the metal electrode.

The WC method and the polarizable electrode model can be combined to construct a hybrid representation of dielectric response at electrochemical interfaces. This unified framework forms the basis for total energy calculations in the ec-MLP model (see Fig. 1). For a given atomic configuration, the positions of Wannier centroids are predicted using an ML model for atomic tensorial

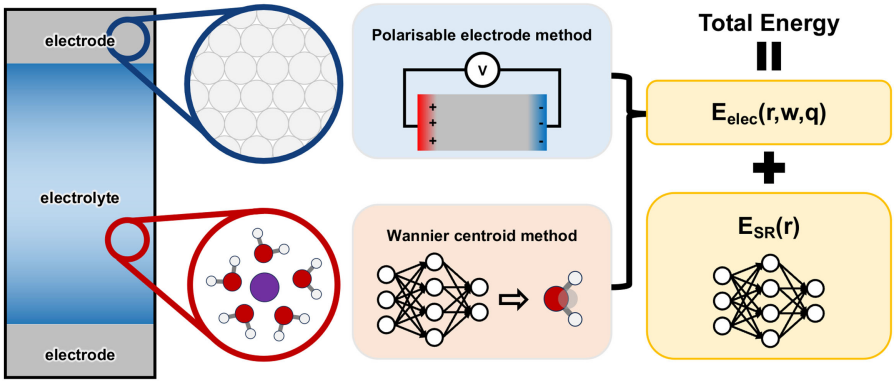

FIG. 1. Schematic illustration of the machine learning model for electrochemistry (ec-MLP). The architecture of the ec-MLP, including the electrostatic and short-range components of the total energy, is shown. The notations are consistent with those used in Eq. (1).

properties [97,104], and the charge distribution in the electrolyte is approximated by point charges located at nuclei and their corresponding WCs. The electrostatic potential computed from this charge distribution, along with the electrostatic boundary conditions and physical constraints (e.g., constant charge or constant potential), determines the atomic charges in the metallic electrode. While charge distributions in our model differ from those obtained in DFT simulations, it is important to note that reproducing the DFT-like charge distribution is not a prerequisite for accurately capturing long-range interactions. As discussed in Ref. [30], well-represented polarization density is sufficient to capture long-range electrostatics interaction, and hence the dielectric properties of our interest. Therefore, the full charge distribution at the interface in our model, comprising both the electrolyte and electrode contributions, enables the evaluation of the long-range electrostatic energy $E_{\mathrm{elec}}(r, w, q)$. The total energy is then expressed as

$$E(r, w, q) = E_{\mathrm{SR}}(r) + E_{\mathrm{elec}}(r, w, q). \tag{1}$$

r and w denote the positions of nuclei and WCs, respectively, and q represents the magnitudes of the charges at these sites. The residual short-range energy $E_{\mathrm{SR}}(r)$ is predicted by an MLP based on local chemical environments [28–30], while the electrostatic term $E_{\mathrm{elec}}(r, w, q)$ is computed as the reciprocal-space contribution in the Ewald summation. In this Letter, the Deep Wannier model [97] and the Siepmann-Sprik model [100] are employed to describe dielectric responses in the electrolyte and the metal electrode, respectively. Nevertheless, the ec-MLP framework is flexible and compatible with other methods of similar purpose.

In the following, the Pt(111)-KF(aq) interface is chosen as the model system to demonstrate the validity of the ec-MLP proposed above. This choice is motivated by the widespread utilization of the Pt(111)-electrolyte interface as the model system in both experimental and computational electrochemistry. Most importantly, it is well-known in the literature that Pt shows a bell-shaped Helmholtz differential capacitance curve [105] caused by dynamic chemisorption of water induced by the applied potential [11]. This phenomenon on Pt highlights the simultaneous importance of electronic structure and molecular dynamics effects, which cannot be accounted for by static DFT or classical molecular dynamics calculation. Therefore, it serves as an excellent model system for validating ec-MLP in comparison with AIMD.

As illustrated in Supplemental Material [41], the ec-MLP is good at predicting energies, atomic forces, and positions of WCs, laying a solid foundation for reproducing the potential-dependent properties of interfaces. In both the training data and the following MD simulations, metal-electrolyte configurations without vacuum layers were used, the details of which are shown in Supplemental Material [41]. Although the DFT data in the training set are generated without an explicit external bias, a wide range of metal slab polarizations (i.e., corresponding surface charge states) are induced self-consistently by the interfacial electrolyte distribution. Consequently, the training dataset effectively captures the dielectric response of the metal surfaces at various surface charges. In the simulations under the potential of zero charge (PZC), the chemisorbed water can be observed in the water density distribution profile in the direction perpendicular to the surface, corresponding to a peak at ~2.3 Å away from the Pt surface [see the insert with red frame in Fig. 2(a)]. Furthermore, the potential-dependent behaviors of the water chemisorption can also be captured. When the potential varies from negative to positive values, the coverage of the chemisorbed water increases, which agrees with the previous AIMD simulations [see Fig. 2(b)]. In addition to water chemisorption, water reorientation at the interface can also be described accurately. The molecular orientation of the chemisorbed water remains almost unchanged. The water molecules located at $2.7 - 4.5$ Å away from the Pt surface,

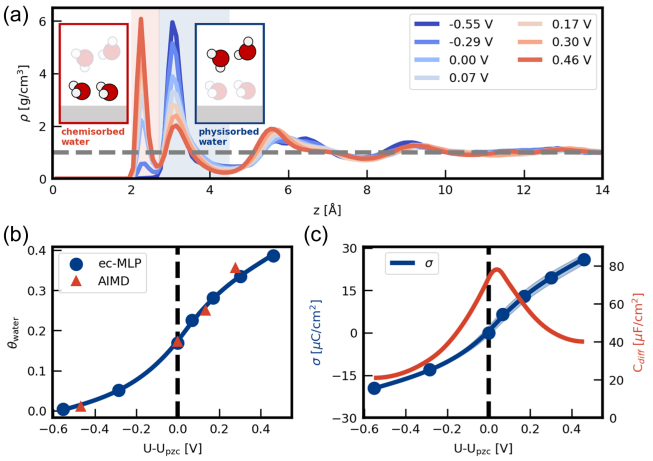

FIG. 2. Structure and capacitance of the Pt-KF interface calculated using the ec-MLP. (a) Water density distribution in the direction perpendicular to the Pt surface under different electrode potentials versus PZC. The zero point in the z coordination is set at the average position of the outermost Pt atoms. The chemisorbed water (red) and the physisorbed water (blue) are identified with the background shadows, the example configurations of which are shown in the insets. The gray dashed line refers to 1 g/cm^3. (b) Potential-dependent coverage of the chemisorbed water. The blue curve and the red triangles represent the results from the simulations with the ec-MLP and from the AIMD simulations [11], respectively. (c) Plots of surface charge density σ and the differential capacitance as a function of potentials versus PZC. The blue curve is the charge density-potential function calculated from the simulations with the ec-MLP, with the uncertainty shown in the blue shadow. The differential capacitance calculated from the first derivative of the blue curve is shown in the red curve.

identified as the physisorbed water, reorientate when changing the electrode potential, leading to a total dipole moment aligning with the electric field. Further details about the potential-dependent orientation of the interfacial water can be found in Supplemental Material [41]. All the results mentioned above, generated from the simulations with the ec-MLP, agree with those from the previous AIMD simulations not only in the qualitative trend but also in the quantitative values [11,106,107].

The accurate description of the potential-dependent water chemisorption and reorientation at the interface makes it possible to reproduce the Helmholtz differential capacitance of the EDL. As shown in Fig. 2(c), the surface charge density-potential function shows the uncertainty smaller than 0.05 V, guaranteeing the statistical accuracy of the differential capacitance curve. Taking the first derivative of the surface charge density-potential function, the differential capacitance can be calculated with its maximum value of $\sim 80\ \mu F/\mathrm{cm}^2$ around the PZC. In the potential windows chosen in this Letter, the differential capacitance curve converges to values of 20 and $40\ \mu F/\mathrm{cm}^2$ at the negative and positive limits, respectively. Overall, the ec-MLP is capable of reproducing the bell shape of the differential capacitance curve, and the capacitance value is in good agreement with the experimental results [105] and the AIMD results [11,108]. Since the bell-shaped capacitance curve can only be captured when taking both electronic structure and molecular dynamics effect into account, this stringent validation strongly shows the suitability and promise of the ec-MLP in simulating electrochemical systems.

Building on the validated ec-MLP, we investigate the dielectric profile at the Pt-water interface. Water in contact with solids shows distinct dielectric behaviors from bulk water, attracting great interest in both experiment and simulation [109]. However, our knowledge of how the dielectric constant changes at such interfaces remains qualitative. While recent MD-based studies have examined dielectric profiles, i.e., spatial distributions of the dielectric constant [110–116], these efforts have focused on inert interfaces. Active systems like Pt-water remain understudied, likely due to the inability of classical force fields to account for interfacial electronic effects and the prohibitive cost of achieving statistical convergence in AIMD simulations. The ec-MLP addresses both challenges, allowing us to compute the dielectric profile at the Pt(111)-water interface for the first time and to uncover the role of electronic polarization in shaping the interfacial dielectric response.

Aiming for the dielectric profile of water at the Pt-water interface, a small perturbing electric field is applied to the model shown in Supplemental Material [41]. Consequently, the dielectric profile can be calculated as shown in Supplemental Material [41]. Particularly, a negative dielectric constant is observed at the region of $2-2.7$ Å, where the chemisorbed water is located. In contrast to the normal dielectric constant ε (i.e., $0 \le \varepsilon^{-1} \le 1$), the negative dielectric constant indicates the overscreening of the electric field by the chemisorbed water layer [115]. The more pronounced the overscreening effect, the more negative the value of the inverse dielectric constant $\varepsilon_{\perp}^{-1}$. The negative dielectric constant agrees with the negative capacitive response of the water chemisorption proposed in the previous work [11]. In contrast, the physisorbed water layer shows a small average dielectric constant of ~ 3, which is close to the dielectric constant used in the traditional EDL model [117].

To estimate the influence of the electronic polarization in water induced by the interface, we calculate a dielectric profile with the water dipole moment set to the bulk value, denoted as the "reference calculation" in the following (see details in Supplemental Material [41]). Based on Fig. 3(a), overscreening of the electric field in the chemisorbed water layer can be attributed to two reasons. On the one hand, the negative values of the red line indicate overscreening stemming from water structuring at the interface. On the other hand, the presence of chemisorption increases the

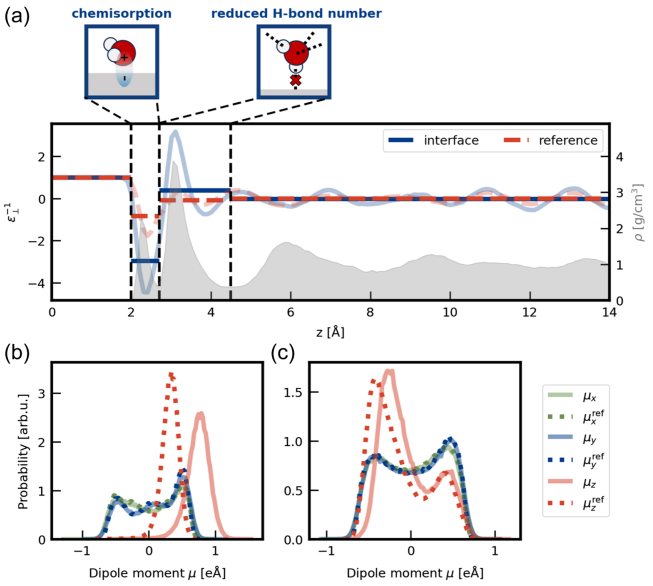

FIG. 3. The dielectric profile of water at the Pt-water interface. (a) The light lines in the background represent the calculated dielectric profiles, including the effects of the intramolecular variations in the electric field. The dark lines in the foreground represent the regional average of the dielectric constant. While the blue lines refer to the calculation at the Pt-water interface, the red line refers to the dielectric profile calculated in the "reference calculation." The shaded area refers to the water density profile at the interface. The two insets on the top illustrate the molecular origins of the electronic polarization in the chemisorbed water and the physisorbed water. Distributions of water dipole moments of the chemisorbed water layer and the physisorbed water layer are shown in (b) and (c), respectively. The subscripts denote the components in the x, y, or z direction. The superscripts of "ref" refer to the results from the reference calculation.

water dipole moment and enhances the overscreening effect, based on the fact that the blue line becomes more negative. The latter can be validated by the probability distribution of chemisorbed water dipole moments. As shown in Fig. 3(b), the molecular dipole moments of chemisorbed water increase in the z direction (i.e., the direction perpendicular to the surface), while those in the x and y directions are almost identical after taking the electronic polarization into account. Overall, the molecular origins of the dielectric property of the chemisorbed water layer shown by our calculation agree with the pictures proposed in previous studies [11,106].

In contrast to the chemisorbed water layer, the dielectric property of the physisorbed water layer is often believed to be mainly influenced by restricted molecular reorientation at the interface rather than electronic polarization [11,109]. Interestingly, a distinct picture can be obtained from Fig. 3(a). In the reference calculation, the physisorbed water layer exhibits an average dielectric constant comparable to the bulk region, which is significantly higher than the result with the effect of electronic polarization. This indicates that the low dielectric constant observed in the physisorbed water layer at the interface is largely influenced by electronic polarization rather than the widely accepted restricted reorientation of water molecules. A picture at the atomic level is revealed in Fig. 3(c), in which the dipole moments of physisorbed water in the z direction become smaller due to the influence of electronic polarization. The reduced water dipole moment can be further rationalized as the results of the lower number of hydrogen bonds [118,119] in the physisorbed water layer compared to the bulk water region. As shown by the inset in Fig. 3(a), the physisorbed water with a reduced dipole points one hydrogen atom toward electrodes and loses one hydrogen-bond donor [107].

To summarize, we introduce the ec-MLP model, which is feasible to describe the dielectric response at the electrode-electrolyte interfaces in a hybrid representation. The ec-MLP shows a high accuracy in predicting not only the water chemisorption but the potential-dependent interfacial water structures and differential capacitances. In particular, the Pt(111)-KF(aq) interface is chosen as the model system, which can only be simulated accurately when both the electronic structure and the molecular dynamics effect are taken into account. The success of ec-MLP in this challenging model system illustrates the feasibility of the method. Furthermore, we extend the timescale of MD simulations to 1 ns with the help of the ec-MLP, and hence are able to calculate the dielectric profile at the Pt-water interface. In the chemisorbed water layer, an overscreening of the electric field is observed due to the synergy of the ordered molecular configurations and the electronic polarization induced by chemisorption. Moreover, the average dielectric constant in the physisorbed water layer illustrates the significant influence of electronic polarization in the absence of chemisorption, which, to the best of our knowledge, has rarely been discussed before. Overall, the insight into the interfacial dielectric properties provided by the ec-MLP is inspiring for further studies of, for example, pH and ion effects, which are highly sensitive to the electronic structure at the interface. Additionally, we anticipate this method will be utilized to investigate some important processes with extended timescales at the electrochemical interface, e.g., electrocatalytic reactions [120,121], formation of solid-electrolyte interphases [122,123], and electrode corrosion [124,125].

Aiming for a wider application of the method, it is worthwhile to discuss how the MLP works under different conditions. At the electrochemical interfaces, there usually exist (electro)chemical reactions, the treatment of which could be different in the MLP. For example, when the chemisorption happens at the interfaces, the electrons of the adsorbate polarize [126], which can be described by the displacements of the WCs in the MLP. As illustrated in Supplemental Material [41], the (partial) charge transfer during the chemisorption can be captured via electron redistribution within the adsorbates under constant potential constraint. In contrast, dealing with the electron transfer in the electrolyte is more complicated. Nevertheless, replacing the Deep Wannier model for electrolytes with the Deep Wannier iterative refinement model [127] can address this limitation.

Finally, we discuss how the ec-MLP can be improved in the future. Currently, only the electrostatic interaction is minimized when solving the atomic charges in the Siepmann-Sprik model with a predefined width of Gaussian charges. The ML-driven QEq method [29,37,40,128,129], where parameters are predicted by ML based on the local chemical environment, can be utilized as a more general and accurate framework to describe the charge redistribution in metal electrodes. On the one hand, the chemical potential of different elements can be taken into account. On the other hand, the Fermi level of the systems can be defined in the framework via the derivative of potential energies with respect to the total electron number. The variation of the total electron number can be reasonably approximated as the variation of the electron number in the metal electrode. The definition of the Fermi level within the ML framework allows us to further calculate or even control the electrode potential with respect to a given reference electrode [130]. Furthermore, while spherical Gaussian distributions are usually used as approximations for charge distributions in the Siepmann-Sprik model, the ML model proposed by Grisafi *et al.* allows reproducing DFT charge distributions in metal electrodes [131,132], and hence is a promising alternative of the Siepmann-Sprik model used in this Letter, especially when such charge distributions are of greater interest.

Acknowledgments—J.-X. Z. gratefully acknowledges Xiamen University and iChEM for a Ph.D. studentship.

J. C. gratefully acknowledges funding from the National Natural Science Foundation of China (Grants No. 22225302, No. 92470201, No. 92461312, No. 22021001, No. 21991151, No. 21991150, No. 92161113, and No. 22411560277), the Fundamental Research Funds for the Central Universities (Grants No. 20720220008, No. 20720220009, and No. 20720220010), Laboratory of AI for Electrochemistry (AI4EC), and Tan Kah Kee Innovation Laboratory (Grants No. RD2023100101 and No. RD2022070501). J.-X. Z. also thanks Dr. Jia-Bo Le, Dr. Xiao-Hui Yang, Dr. Katharina Doblhoff-Dier, and Dr. Jun Huang for their helpful discussions. The authors thank Dr. Linfeng Zhang, Dr. Han Wang, and DP community for helpful discussions and technical support.

[1] Z. Zhang, C. Feng, C. Liu, M. Zuo, L. Qin, X. Yan, Y. Xing, H. Li, R. Si, S. Zhou, and J. Zeng, Nat. Commun. **11**, 1215 (2020).
[2] M. C. Leech and K. Lam, Nat. Rev. Chem. **6**, 275 (2022).
[3] J. K. Nørskov, J. Rossmeisl, A. Logadottir, L. Lindqvist, J. R. Kitchin, T. Bligaard, and H. Jónsson, J. Phys. Chem. B **108**, 17886 (2004).
[4] J. T. S. Irvine, D. Neagu, M. C. Verbraeken, C. Chatzichristodoulou, C. Graves, and M. B. Mogensen, Nat Energy **1**, 15014 (2016).
[5] J. B. Goodenough and K.-S. Park, J. Am. Chem. Soc. **135**, 1167 (2013).
[6] Chinese Society of Electrochemistry, J. Electrochem. **30**, 2024121 (2024).
[7] I. Ledezma-Yanez, W. D. Z. Wallace, P. Sebastián-Pascual, V. Climent, J. M. Feliu, and M. T. M. Koper, Nat. Energy **2**, 17031 (2017).
[8] P. Li, Y. Jiang, Y. Hu, Y. Men, Y. Liu, W. Cai, and S. Chen, Nat. Catal. **5**, 900 (2022).
[9] T. Wang, Y. Zhang, B. Huang, B. Cai, R. R. Rao, L. Giordano, S.-G. Sun, and Y. Shao-Horn, Nat. Catal. **4**, 753 (2021).
[10] T. L. Maier, L. B. T. de Kam, M. Golibrzuch, T. Angerer, M. Becherer, and K. Krischer, ChemElectroChem **11**, e202400109 (2024).
[11] J.-B. Le, Q.-Y. Fan, J.-Q. Li, and J. Cheng, Sci. Adv. **6**, eabb1219 (2020).
[12] X.-H. Yang, Y.-B. Zhuang, J.-X. Zhu, J.-B. Le, and J. Cheng, WIREs Comput. Mol. Sci. **12**, e1559 (2021).
[13] J. Behler and M. Parrinello, Phys. Rev. Lett. **98**, 146401 (2007).
[14] A. P. Bartók, M. C. Payne, R. Kondor, and G. Csányi, Phys. Rev. Lett. **104**, 136403 (2010).
[15] S. Batzner, A. Musaelian, L. Sun, M. Geiger, J. P. Mailoa, M. Kornbluth, N. Molinari, T. E. Smidt, and B. Kozinsky, Nat. Commun. **13**, 2453 (2022).
[16] J. Zeng *et al.*, J. Chem. Phys. **159**, 054801 (2023).
[17] W. Jia, H. Wang, M. Chen, D. Lu, L. Lin, R. Car, E. Weinan, and L. Zhang, in *SC20: International Conference for High Performance Computing, Networking, Storage and Analysis* (IEEE, Atlanta, GA, 2020).
[18] P. Mo, C. Li, D. Zhao, Y. Zhang, M. Shi, J. Li, and J. Liu, npj Comput. Mater. **8**, 107 (2022).
[19] S. Ma, S.-D. Huang, and Z.-P. Liu, Nat. Catal. **2**, 671 (2019).
[20] Y. Yang, Z. Guo, A. J. Gellman, and J. R. Kitchin, J. Phys. Chem. C **126**, 1800 (2022).
[21] F.-Q. Gong, Y.-P. Liu, Y. Wang, W. E, Z.-Q. Tian, and J. Cheng, Angew. Chem. **136**, e202405379 (2024).
[22] J. Lan, V. Kapil, P. Gasparotto, M. Ceriotti, M. Iannuzzi, and V. V. Rybkin, Nat. Commun. **12**, 766 (2021).
[23] A. P. Bartók, R. Kondor, and G. Csányi, Phys. Rev. B **87**, 184115 (2013).
[24] L. Zhang, J. Han, H. Wang, W. A. Saidi, R. Car, and E. Weinan, in Advances in Neural Information Processing Systems (2018), Vol. **2018**, pp. 4436–4446, arXiv:1805.09003.
[25] J. Fiedler, M. Boström, C. Persson, I. Brevik, R. Corkery, S. Y. Buhmann, and D. F. Parsons, J. Phys. Chem. B **124**, 3103 (2020).
[26] C. Zhang, J. Chem. Phys. **148**, 156101 (2018).
[27] C. Zhang, M. F. Calegari Andrade, Z. K. Goldsmith, A. S. Raman, Y. Li, P. M. Piaggi, X. Wu, R. Car, and A. Selloni, Nat. Commun. **15**, 10270 (2024).
[28] N. Artrith, T. Morawietz, and J. Behler, Phys. Rev. B **83**, 153101 (2011).
[29] T. Dufils, L. Knijff, Y. Shao, and C. Zhang, J. Chem. Theory Comput. **19**, 5199 (2023).
[30] L. Zhang, H. Wang, M. C. Muniz, A. Z. Panagiotopoulos, R. Car, and W. E, J. Chem. Phys. **156**, 1024107 (2022).
[31] A. Gao and R. C. Remsing, Nat. Commun. **13**, 1572 (2022).
[32] A. Grisafi and M. Ceriotti, J. Chem. Phys. **151**, 204105 (2019).
[33] A. M. Lewis, P. Lazzaroni, and M. Rossi, J. Chem. Phys. **159**, 014103 (2023).
[34] S. Falletta, A. Cepellotti, C. W. Tan, A. Johansson, A. Musaelian, C. J. Owen, and B. Kozinsky, Nat. Commun. **16**, 4031 (2025).
[35] K. Joll, P. Schienbein, K. M. Rosso, and J. Blumberger, Nat. Commun. **15**, 8192 (2024).
[36] S. A. Ghasemi, A. Hofstetter, S. Saha, and S. Goedecker, Phys. Rev. B **92**, 045131 (2015).
[37] T. W. Ko, J. A. Finkler, S. Goedecker, and J. Behler, J. Chem. Theory Comput. **19**, 3567 (2023).
[38] T. Verstraelen, P. W. Ayers, V. Van Speybroeck, and M. Waroquier, J. Chem. Phys. **138**, 074108 (2013).
[39] T. Verstraelen and P. Bultinck, Spectrochim. Acta, Part A **136**, 76 (2015).
[40] Y. Shao, L. Andersson, L. Knijff, and C. Zhang, Electron. Struct. **4**, 014012 (2022).
[41] See Supplemental Material at http://link.aps.org/supplemental/10.1103/48ct-3jxm for method details and tests of the ec-MLP, which includes Refs. [42–106].
[42] K. Schwarz and R. Sundararaman, Surf. Sci. Rep. **75**, 100492 (2020).
[43] S. Grimme, J. Antony, S. Ehrlich, and H. Krieg, J. Chem. Phys. **132**, 154104 (2010).
[44] J. Huang, JACS Au **3**, 550 (2023).
[45] T. Pajkossy, Solid State Ionics **176**, 1997 (2005).
[46] I. Souza, J. Íñiguez, and D. Vanderbilt, Phys. Rev. Lett. **89**, 117602 (2002).

[47] F. Giustino and A. Pasquarello, Phys. Rev. B **71**, 144104 (2005).
[48] S. K. Natarajan and J. Behler, Phys. Chem. Chem. Phys. **18**, 28704 (2016).
[49] R. Jinnouchi, F. Karsai, C. Verdi, and G. Kresse, J. Chem. Phys. **154**, 094107 (2021).
[50] T. D. Kühne *et al.*, J. Chem. Phys. **152**, 194103 (2020).
[51] R. Resta and S. Sorella, Phys. Rev. Lett. **82**, 370 (1999).
[52] J. K. Nørskov, T. Bligaard, A. Logadottir, J. R. Kitchin, J. G. Chen, S. Pandelov, and U. Stimming, J. Electrochem. Soc. **152**, J23 (2005).
[53] T. Darden, D. York, and L. Pedersen, J. Chem. Phys. **98**, 10089 (1993).
[54] Y. Chao, H. Li, T.-W. Jiang, J.-A. Huang, X.-Y. Ma, K. Jiang, and W.-B. Cai, Curr. Opin. Electrochem. **46**, 101509 (2024).
[55] W. Sheng, Z. Zhuang, M. Gao, J. Zheng, J. G. Chen, and Y. Yan, Nat. Commun. **6**, 5848 (2015).
[56] K. Ojha, K. Doblhoff-Dier, and M. T. M. Koper, Proc. Natl. Acad. Sci. U.S.A. **119**, e2116016119 (2022).
[57] P. Grosse, A. Yoon, C. Rettenmaier, A. Herzog, S. W. Chee, and B. Roldan Cuenya, Nat. Commun. **12**, 6736 (2021).
[58] X. Chen, L. P. Granda-Marulanda, I. T. McCrum, and M. T. M. Koper, Chem. Sci. **11**, 1703 (2020).
[59] C.-Y. Li, J.-B. Le, Y.-H. Wang, S. Chen, Z.-L. Yang, J.-F. Li, J. Cheng, and Z.-Q. Tian, Nat. Mater. **18**, 697 (2019).
[60] N. G. Hörmann, S. D. Beinlich, and K. Reuter, J. Phys. Chem. C **128**, 5524 (2024).
[61] K. Doblhoff-Dier and M. T. Koper, Curr. Opin. Electrochem. **39**, 101258 (2023).
[62] X. Wang, J. Li, L. Yang, F. Chen, Y. Wang, J. Chang, J. Chen, W. Feng, L. Zhang, and K. Yu, J. Chem. Theory Comput. **19**, 5897 (2023).
[63] S. Goedecker, M. Teter, and J. Hutter, Phys. Rev. B **54**, 1703 (1996).
[64] P. Umari and A. Pasquarello, Phys. Rev. Lett. **89**, 157602 (2002).
[65] J. M. Feliu and E. Herrero, EES Catal. **2**, 399 (2024).
[66] H. Liu, Z. Qi, and L. Song, J. Phys. Chem. C **125**, 24289 (2021).
[67] L. J. V. Ahrens-Iwers, M. Janssen, S. R. Tee, and R. H. Meißner, J. Chem. Phys. **157**, 084801 (2022).
[68] J. P. Perdew, K. Burke, and M. Ernzerhof, Phys. Rev. Lett. **77**, 3865 (1996).
[69] L. Zhang and J. Huang, Curr. Opin. Electrochem. **42**, 101419 (2023).
[70] R. W. Nunes and X. Gonze, Phys. Rev. B **63**, 155107 (2001).
[71] A. Groß and S. Sakong, Chem. Rev. **122**, 10746 (2022).
[72] J. VandeVondele, M. Krack, F. Mohamed, M. Parrinello, T. Chassaing, and J. Hutter, Comput. Phys. Commun. **167**, 103 (2005).
[73] S. Ringe, N. G. Hörmann, H. Oberhofer, and K. Reuter, Chem. Rev. **122**, 10777 (2021).
[74] S. K. Reed, O. J. Lanning, and P. A. Madden, J. Chem. Phys. **126**, 084704 (2007).
[75] A. P. Thompson, H. M. Aktulga, R. Berger, D. S. Bolintineanu, W. M. Brown, P. S. Crozier, P. J. in 't Veld, A. Kohlmeyer, S. G. Moore, T. D. Nguyen, R. Shan, M. J. Stevens, J. Tranchida, C. Trott, and S. J. Plimpton, Comput. Phys. Commun. **271**, 108171 (2022).
[76] M. Stengel, N. A. Spaldin, and D. Vanderbilt, Nat. Phys. **5**, 304 (2009).
[77] C. Hartwigsen, S. Goedecker, and J. Hutter, Phys. Rev. B **58**, 3641 (1998).
[78] R. Rizo, E. Sitta, E. Herrero, V. Climent, and J. M. Feliu, Electrochim. Acta **162**, 138 (2015).
[79] F. Wang and J. Cheng, J. Chem. Phys. **157**, 024103 (2022).
[80] K. Bian, C. Gerber, A. J. Heinrich, D. J. Müller, S. Scheuring, and Y. Jiang, Nat. Rev. Methods Primers **1**, 36 (2021).
[81] Y. Zhang, H. Wang, W. Chen, J. Zeng, L. Zhang, H. Wang, and W. E, Comput. Phys. Commun. **253**, 107206 (2020).
[82] S. Shin and A. P. Willard, J. Phys. Chem. B **122**, 6781 (2018).
[83] J.-B. Le, X.-H. Yang, Y.-B. Zhuang, M. Jia, and J. Cheng, J. Phys. Chem. Lett. **12**, 8924 (2021).
[84] C. Zhang, J. Hutter, and M. Sprik, J. Phys. Chem. Lett. **7**, 2696 (2016).
[85] B. E. Conway and B. Pierozynski, J. Electroanal. Chem. **622**, 10 (2008).
[86] X. Chen, I. T. McCrum, K. A. Schwarz, M. J. Janik, and M. T. M. Koper, Angew. Chem., Int. Ed. **56**, 15025 (2017).
[87] J. K. Staffa, L. Lorenz, M. Stolarski, D. H. Murgida, I. Zebger, T. Utesch, J. Kozuch, and P. Hildebrandt, J. Phys. Chem. C **121**, 22274 (2017).
[88] D. Frenkel and B. Smit, *Understanding Molecular Simulation: From Algorithms to Applications*, 2nd ed., Computational Science Series Vol. 1 (Academic Press, San Diego, 2002).
[89] C. Malosso, L. Zhang, R. Car, S. Baroni, and D. Tisi, npj Comput. Mater. **8**, 139 (2022).
[90] T. A. Pham, T. Ogitsu, E. Y. Lau, and E. Schwegler, J. Chem. Phys. **145**, 154501 (2016).
[91] S. Blazquez, J. L. F. Abascal, J. Lagerweij, P. Habibi, P. Dey, T. J. H. Vlugt, O. A. Moultos, and C. Vega, J. Chem. Theory Comput. **19**, 5380 (2023).
[92] F. Giustino and A. Pasquarello, Phys. Rev. B **71**, 144104 (2005).
[93] Z. Wang, M. Chen, J. Wu, X. Ji, L. Zeng, J. Peng, J. Yan, A. A. Kornyshev, B. Mao, and G. Feng, Phys. Rev. Lett. **134**, 046201 (2025).
[94] W. Schmickler, Chem. Rev. **96**, 3177 (1996).
[95] W. J. Mortier, S. K. Ghosh, and S. Shankar, J. Am. Chem. Soc. **108**, 4315 (1986).
[96] C. Merlet, B. Rotenberg, P. A. Madden, P.-L. Taberna, P. Simon, Y. Gogotsi, and M. Salanne, Nat. Mater. **11**, 306 (2012).
[97] L. Zhang, M. Chen, X. Wu, H. Wang, W. E, and R. Car, Phys. Rev. B **102**, 041121(R) (2020).
[98] J.-X. Zhu, J. Cheng, and K. Doblhoff-Dier, J. Chem. Phys. **162**, 24702 (2025).
[99] I. L. Geada, H. Ramezani-Dakhel, T. Jamil, M. Sulpizi, and H. Heinz, Nat. Commun. **9**, 716 (2018).
[100] J. I. Siepmann and M. Sprik, J. Chem. Phys. **102**, 511 (1995).
[101] H. Nakano and H. Sato, J. Chem. Phys. **151**, 164123 (2019).
[102] L. Zeng, J. Peng, J. Zhang, X. Tan, X. Ji, S. Li, and G. Feng, J. Chem. Phys. **159**, 91001 (2023).

[103] D. Golze, M. Iannuzzi, M.-T. Nguyen, D. Passerone, and J. Hutter, J. Chem. Theory Comput. **9**, 5086 (2013).
[104] A. Grisafi, D. M. Wilkins, G. Csányi, and M. Ceriotti, Phys. Rev. Lett. **120**, 036002 (2018).
[105] T. Pajkossy and D. Kolb, Electrochem. Comm. **5**, 283 (2003).
[106] J. Le, M. Iannuzzi, A. Cuesta, and J. Cheng, Phys. Rev. Lett. **119**, 016801 (2017).
[107] J. Le, A. Cuesta, and J. Cheng, J. Electroanal. Chem. **819**, 87 (2018).
[108] X. Wang, Y. Wang, Y. Kuang, and J.-B. Le, J. Phys. Chem. Lett. **14**, 7833 (2023).
[109] L. Fumagalli, A. Esfandiar, R. Fabregas, S. Hu, P. Ares, A. Janardanan, Q. Yang, B. Radha, T. Taniguchi, K. Watanabe, G. Gomila, K. S. Novoselov, and A. K. Geim, Science **360**, 1339 (2018).
[110] D. J. Bonthuis, S. Gekle, and R. R. Netz, Phys. Rev. Lett. **107**, 166102 (2011).
[111] D. J. Bonthuis, S. Gekle, and R. R. Netz, Langmuir **28**, 7679 (2012).
[112] F. Deißenbeck, C. Freysoldt, M. Todorova, J. Neugebauer, and S. Wippermann, Phys. Rev. Lett. **126**, 136803 (2021).
[113] J.-F. Olivieri, J. T. Hynes, and D. Laage, J. Phys. Chem. Lett. **12**, 4319 (2021).
[114] P. Loche, L. Scalfi, M. Ali Amu, O. Schullian, D. J. Bonthuis, B. Rotenberg, and R. R. Netz, J. Chem. Phys. **157**, 094707 (2022).
[115] B. Tran, Y. Zhou, M. J. Janik, and S. T. Milner, Phys. Rev. Lett. **131**, 248001 (2023).
[116] F. Deißenbeck and S. Wippermann, J. Chem. Theory Comput. **19**, 1035 (2023).
[117] B. E. Conway, J. O. Bockris, and I. A. Ammar, Trans. Faraday Soc. **47**, 756 (1951).
[118] J. K. Gregory, D. C. Clary, K. Liu, M. G. Brown, and R. J. Saykally, Science **275**, 814 (1997).
[119] D. D. Kemp and M. S. Gordon, J. Phys. Chem. A **112**, 4885 (2008).
[120] T. Cheng, H. Xiao, and W. A. Goddard, J. Phys. Chem. Lett. **6**, 4767 (2015).
[121] C. Choi, S. Kwon, T. Cheng, M. Xu, P. Tieu, C. Lee, J. Cai, H. M. Lee, X. Pan, X. Duan, W. A. Goddard, and Y. Huang, Nat. Catal. **3**, 804 (2020).
[122] A. Wang, S. Kadam, H. Li, S. Shi, and Y. Qi, npj Comput. Mater. **4**, 15 (2018).
[123] X. Qin, A. Bhowmik, T. Vegge, and I. E. Castelli, ACS Appl. Mater. Interfaces **16**, 29347 (2024).
[124] S. Surendralal, M. Todorova, M. W. Finnis, and J. Neugebauer, Phys. Rev. Lett. **120**, 246801 (2018).
[125] N. Arulmozhi, T. J. P. Hersbach, and M. T. M. Koper, Proc. Natl. Acad. Sci. U.S.A. **117**, 32267 (2020).
[126] W. Schmickler and E. Santos, *Interfacial Electrochemistry* (Springer, Berlin Heidelberg, 2010).
[127] R. Gao, Y. Li, and R. Car, Phys. Chem. Chem. Phys. **26**, 23080 (2024).
[128] A. K. Rappe and W. A. Goddard, J. Phys. Chem. **95**, 3358 (1991).
[129] D. M. York and W. Yang, J. Chem. Phys. **104**, 159 (1996).
[130] J. Cheng and M. Sprik, Phys. Chem. Chem. Phys. **14**, 11245 (2012).
[131] A. Grisafi, A. Bussy, M. Salanne, and R. Vuilleumier, Phys. Rev. Mater. **7**, 125403 (2023).
[132] A. Grisafi and M. Salanne, J. Chem. Phys. **161**, 024109 (2024).